

Benchmarking Multi-modal Semantic Segmentation under Sensor Failures: Missing and Noisy Modality Robustness

Chenfei Liao^{1,*} Kaiyu Lei^{2,*} Xu Zheng^{1,3,†} Junha Moon¹ Zhixiong Wang¹
Yixuan Wang¹ Danda Pani Paudel³ Luc Van Gool³ Xuming Hu^{1,4,‡}

¹HKUST(GZ) ²XJTU ³INSAIT, Sofia University “St. Kliment Ohridski”, ⁴CSE, HKUST

Abstract

Multi-modal semantic segmentation (MMSS) addresses the limitations of single-modality data by integrating complementary information across modalities. Despite notable progress, a significant gap persists between research and real-world deployment due to variability and uncertainty in multi-modal data quality. Robustness has thus become essential for practical MMSS applications. However, the absence of standardized benchmarks for evaluating robustness hinders further advancement. To address this, we first survey existing MMSS literature and categorize representative methods to provide a structured overview. We then introduce a robustness benchmark that evaluates MMSS models under three scenarios: Entire-Missing Modality (EMM), Random-Missing Modality (RMM), and Noisy Modality (NM). From a probabilistic standpoint, we model modality failure under two conditions: (1) all damaged combinations are equally probable; (2) each modality fails independently following a Bernoulli distribution. Based on these, we propose four metrics— $mIoU_{EMM}^{Avg}$, $mIoU_{EMM}^E$, $mIoU_{RMM}^{Avg}$, and $mIoU_{RMM}^E$ —to assess model robustness under EMM and RMM. This work provides the first dedicated benchmark for MMSS robustness, offering new insights and tools to advance the field. Source code is available at <https://github.com/Chenfei-Liao/Multi-Modal-Semantic-Segmentation-Robustness-Benchmark>.

1. Introduction

Multi-modal semantic segmentation has emerged as a critical task in computer vision, leveraging diverse sensor inputs to produce more accurate and reliable pixel-wise classification results [20, 43]. By fusing information from complementary modalities such as RGB, depth, LiDAR,

*These authors have equal contributions.

†Project lead.

‡Corresponding author.

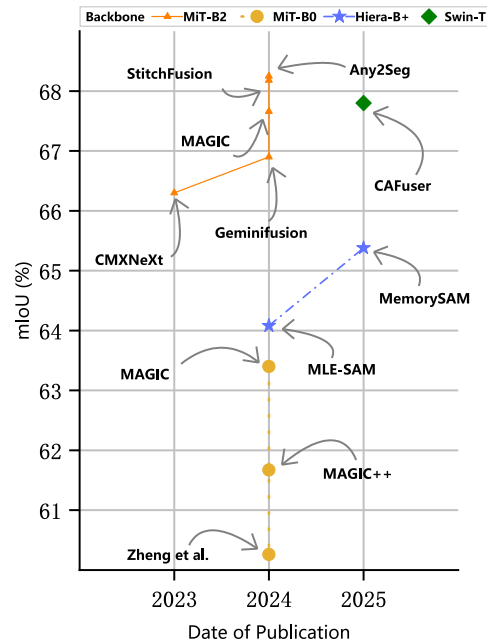


Figure 1. History of MMSS methods.

thermal, and event, multi-modal systems are capable of overcoming the limitations inherent to single-modality approaches [9, 26, 27, 45]. Such integration is particularly beneficial in autonomous driving, robotics, and surveillance applications, where harsh environmental challenges like low-light and adverse weather conditions may severely degrade the performance of individual sensors [17, 19, 29, 42].

Despite these advantages, deploying multi-modal systems in real-world environments presents critical robustness challenges that are often underexplored in existing research [41]. In practice, sensor data may be incomplete, degraded, or entirely unavailable. For example, RGB cameras may struggle in low-light or foggy conditions; LiDAR sensors can produce sparse or noisy point clouds in heavy rain; thermal cameras are sensitive to ambient temperature variations; and event cameras may fail in low-contrast

scenes [6, 12, 14, 31, 32, 35, 39]. These scenarios illustrate the pressing need to evaluate and improve the robustness of multi-modal semantic segmentation (MMSS) models under real-world conditions.

To systematically address these issues, robustness in MMSS can be classified into three representative failure scenarios. First, Entire-Missing Modality (EMM) refers to the complete loss of a sensor’s input, requiring the model to perform without that modality [18, 46, 47]. Second, Random-Missing Modality (RMM) captures intermittent or partial sensor failures that cause unpredictable data absence. Third, Noisy Modality (NM) describes cases where sensors continue to provide input, but the data is degraded or corrupted due to environmental or hardware factors [48, 51]. While some studies have explored EMM and NM, RMM—despite its high practical relevance—remains largely underexamined in the current literature.

In this paper, we present a comprehensive benchmark to systematically evaluate modality robustness in Multi-Modal Semantic Segmentation (MMSS). Our study begins by surveying and categorizing existing MMSS methods according to their architectural design principles and fusion strategies [40, 43]. We identify three primary approaches: (1) RGB-centric methods that use other modalities as supplementary information [40]; (2) Equal-contribution methods that treat all modalities with uniform importance [15]; (3) Adaptive-selection methods that dynamically determine modality contributions [13, 48]. We then evaluate these methods under our three robustness scenarios (EMM, RMM, and NM) using the DELIVER dataset [40], which provides multi-modal acquired data under diverse environmental conditions. Our systematic evaluation reveals strengths and weaknesses in current approaches and illuminates promising directions for more robust systems.

Our contributions can be concluded as follows: (I) We comprehensively collect the works related to the multi-modal semantic segmentation task and categorize them systematically. (II) We build a robust benchmark for the multi-modal semantic segmentation task, including 3 scenarios: EMM, RMM, and NM. (III) From a statistical point of view, we propose new metrics to evaluate the performance of the model in both EMM and RMM cases.

2. Related work

2.1. Related Surveys and Benchmarks

The development of intelligent vision sensors has sparked extensive research on multi-modal semantic segmentation, resulting in several surveys and benchmarks in this field. **The Surveys** on multi-modal semantic segmentation provide a comprehensive summary of existing methods, covering both bi-modal semantic segmentation and multi-modal semantic segmentation. For instance, [26, 27, 45] focus

Table 1. Comparison of modality robustness across MMSS methods. RMM: Random-Missing Modality; EMM: Entire-Missing Modality; NM: Noisy Modality.

Work	Publication	RMM	EMM	NM
MCubesNet [15]	CVPR2022	✗	✗	✗
TokenFusion [30]	CVPR2022	✗	✗	✗
CMXNeXt [40]	CVPR2023	✗	✗	✗
GeminiFusion [10]	ICML2024	✗	✗	✗
MAGIC [48]	ECCV2024	✗	✓	✓
Any2Seg [47]	ECCV2024	✗	✓	✓
FPT [18]	IV2024	✗	✓	✓
MAGIC++ [46]	Arxiv2024	✗	✓	✓
MLE-SAM [51]	Arxiv2024	✗	✓	✓
AnySeg [49]	Arxiv2024	✗	✓	✗
StitchFusion [13]	Arxiv2024	✗	✗	✗
CAFuser [2]	RAL2025	✗	✗	✗
MemorySAM [16]	Arxiv2025	✗	✗	✗

on the various modality combinations such as RGB-Depth, RGB-Thermal, RGB-Event, and so on. As to the multi-modal semantic segmentation, [43] offers an in-depth review of fusion strategies for handling multi-modal data. Moreover, [9] concentrates on autonomous driving scenarios, providing insights from the perspective of real-world applications. **The Benchmarks** offer a fair comparison of advanced methods, providing effective performance measurements. Currently, DELIVER [40], MUSES [1], and MCubes [15] are the most common benchmarks for multi-modal semantic segmentation, enabling researchers to test their methods under various modality combinations.

The relevant surveys and benchmarks lay their emphasis on the accuracy of semantic segmentation models with multi-modal settings. While, in real-world applications, the multi-sensor systems will not permanently be as perfect as assumed. Besides accuracy, the robustness of multi-modal semantic segmentation models also plays a crucial role to the entire system, especially when sensors are disturbed or malfunctioning. *However, building a robustness benchmark of multi-modal semantic segmentation for multi-sensor systems remains a research gap. Our work is the first attempt to address this gap, hoping to bring new insights to the multi-modal semantic segmentation task.*

2.2. Multi-modal Semantic Segmentation

As a vital task in the computer vision field, semantic segmentation aims to allocate a class for each pixel [20]. Due to the lack of multi-modal datasets, previous research mainly focuses on the uni-modality [8, 11, 21–24, 28, 33, 37, 38] or bi-modality such as RGB-Depth [3–5, 25, 36], RGB-Thermal [6, 14, 31, 44, 50], RGB-Event [12, 32, 35, 39],

and so on. With the development of vision sensor techniques and relevant multi-modal datasets, several multi-modal semantic segmentation models [13, 15, 40, 48] are proposed to better cope with real-world requirements, which is shown in Fig.1. From the perspective of modality contribution, existing multi-modal semantic segmentation models can be classified into 3 types. ① Take RGB as the main contributor [40]. CMXNet [40] designs a Self-Query Hub to choose informative features from other modalities, which serve as supplements to the primary RGB information. ② Take all modalities as equal contributors [2, 10, 13, 30, 51, 51].MCubeSNet [15] fuses multi-level features of different modalities in a concatenation way. ③ Find the main contributor adaptively [16, 46–49]. Most representatively, MAGIC [48] determines the main contributor based on the similarity between each modality’s features and the aggregated features. From these three design paradigms, several initial conjectures can be given. Firstly, Type① is supposed to be more sensitive to the RGB modality. Its robustness relies on the stability of the RGB camera, which means the vulnerability of the model to RGB-in-friendly environments such as at night, cloudy, and so on. Secondly, Type② is supposed to be moderately robust. Such models will not be greatly degraded by the interference or absence of a certain modality. Thirdly, Type③ is supposed to be equipped with the best modality robustness. The adaptive selection of the main contributor decreases the influence of the bad modality on the entire model. The experiments and further discussions are shown in Section 4.2 and Section 4.3.

2.3. Modality Robustness

Research endeavors have focused on designing robust multi-modal frameworks to handle the modality-incomplete data [18, 46–49, 51]. Current works mainly focus on the entire-missing modality (EMM) condition and noisy modality (NM) condition as shown in Table 1, which clearly compares how different methods emphasize modality robustness. In more detail, Any2Seg [47] attempts to utilize knowledge distillation from MVLMs to solve modality-agnostic segmentation. MAGIC [48] and MAGIC++ [46] attempt to evaluate each modality’s contribution to facilitate efficient cross-modal fusion, especially when faced with EMM and NM. However, as in Table 1, each study targets different aspects of modality robustness. Thus, we hope to establish a benchmark that evaluates how existing methods perform when dealing with the modality robustness problem. In addition, while most current methods focus on EMM and NM, they often skip random-missing modality (RMM) scenarios, which are closer to the real-world application. Our proposed benchmark will include RMM, EMM, and NM conditions along with all the existing open-source multi-modal semantic segmentation methods, attempting to

bring new insights for future works.

3. Our Benchmarks

3.1. Evaluation Datasets

In this research, we use the DELIVER [40] multi-modal dataset to evaluate semantic segmentation models. The dataset includes Depth, LiDAR, Multiple Views, Events, and RGB images, captured under five weather conditions (cloudy, foggy, night-time, rainy, and sunny). Each weather condition also includes five corner cases: Motion Blur (MB), Over-Exposure (OE), Under-Exposure (UE), LiDAR-Jitter (LJ), and Event Low-resolution (EL), which reflect real-world sensor performance challenges.

The DELIVER [40] dataset was generated using the CARLA simulator [7], a widely used open-source platform for autonomous driving research. It is specifically designed to simulate diverse and dynamic urban driving environments, ensuring that models can be evaluated under a wide range of practical, real-world conditions. The dataset provides six views per sample, each containing four modalities and two types of labels (semantic and instance segmentation), creating a rich multi-sensor setup. This makes the dataset ideal for evaluating model robustness under the context of autonomous driving, where conditions such as varying weather, sensor degradation, and complex environments are common. With 25 semantic classes, the DELIVER[40] dataset enables a comprehensive evaluation of model performance across diverse segmentation tasks. Its carefully curated collection of data, encompassing diverse environmental challenges, serves as a valuable benchmark for assessing how well segmentation models generalize to real-world autonomous driving scenarios. The dataset’s unique combination of multi-modal data and real-world simulations makes it particularly well-suited for evaluating the performance and robustness of models under conditions that closely resemble those encountered in actual deployments.

3.2. Evaluation Methods

3.2.1. Entire-Missing Modality

In real-world applications, multi-modal systems often face sensor damage. The most severe case is a complete failure of the sensors, which means that the corresponding modal data is entirely zeroed out. For instance, when the depth camera is entirely broken in an intelligent vehicle, all depth data becomes unavailable. To simulate this situation, we set the missing modalities’ data to zero and then make the entire data go through the trained model based on the full modality combination. Let the complete modality set as $M = \{m_1, m_2, m_3, \dots, m_n\}$ and represent the missing modality combinations as $\{M'_1, M'_2, \dots, M'_N\} \subseteq M$, where each M'_i is a combination obtained by removing certain modalities from the complete modality combination

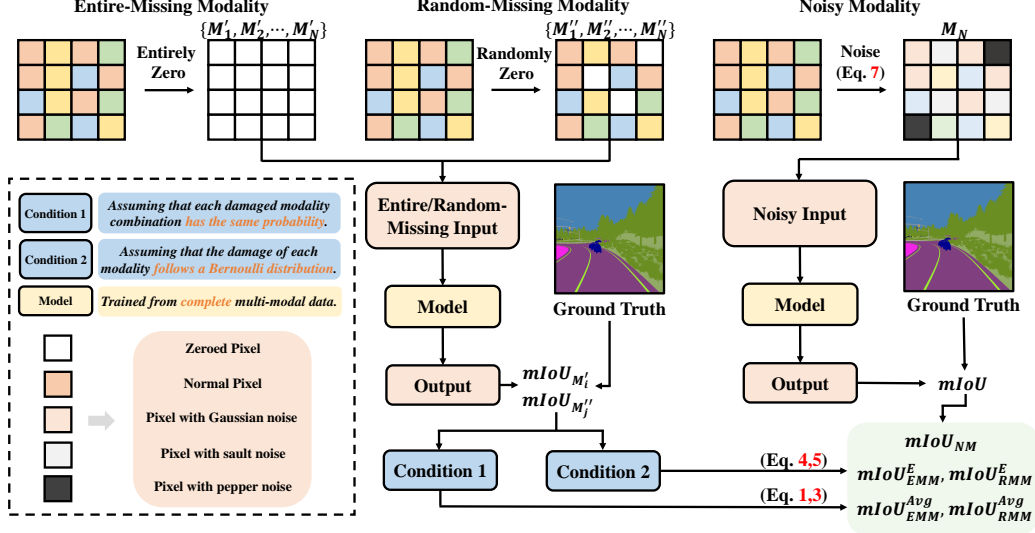


Figure 2. Framework of our multi-modal semantic segmentation robustness benchmark.

M , and N denotes the number of different M' .

To evaluate the model's performance under missing modalities, we first define $mIoU_{EMM}$ as the mean intersection over union (IoU) for the missing modality combinations, as shown in Eq. 1, where $mIoU_{M'_i}^{Avg}$ represents the validation mIoU for the corresponding missing modality combination M'_i , using the model weights trained on the complete modality combination.

$$mIoU_{EMM}^{Avg} = \frac{1}{N} \sum_{i=1}^N mIoU_{M'_i}. \quad (1)$$

Furthermore, to consider the case of equal damage probabilities across all modalities, we further define $mIoU_{EMM}^E$ as the expected mIoU under the assumption of equal damage probabilities for each individual modality. Assuming that the damage of each modality follows a Bernoulli distribution with a probability p , we can represent the expected mIoU for all combinations of missing modalities. The probability of a specific combination of k modalities being damaged while the remaining $n - k$ modalities are not damaged can be expressed using the binomial distribution. Specifically, for a combination M'_i that includes k damaged modalities, the probability $P(M'_i^k)$ is given by Eq. 2. $mIoU_{EMM}^E$ can then be calculated as Eq. 3, where M'_i^k is a combination obtained by removing k modalities from the complete modality combination M , and $\binom{n}{k}$ denotes the number of ways to choose k modalities from n . The example of the R-D-E-L modality combination is shown in Table 2.

$$P_p(M'_i^k) = p^k \cdot (1 - p)^{n-k}, \quad (2)$$

$$mIoU_{EMM}^E(p) = \sum_{k=0}^{n-1} \sum_{i=1}^{\binom{n}{k}} P_p(M'_i^k) \cdot mIoU_{M'_i}. \quad (3)$$

Table 2. All combinations of missing modalities and their probabilities under the R-D-E-L modality combination.

Modality Combination	Probability P
RGB-Depth-Event-LiDAR	$(1 - p)^4$
RGB-Depth-Event	$p(1 - p)^3$
RGB-Depth-LiDAR	$p(1 - p)^3$
RGB-Event-LiDAR	$p(1 - p)^3$
Depth-Event-LiDAR	$p(1 - p)^3$
RGB-Depth	$p^2(1 - p)^2$
RGB-Event	$p^2(1 - p)^2$
RGB-LiDAR	$p^2(1 - p)^2$
Depth-Event	$p^2(1 - p)^2$
Depth-LiDAR	$p^2(1 - p)^2$
Event-LiDAR	$p^2(1 - p)^2$
RGB	$p^3(1 - p)$
Depth	$p^3(1 - p)$
Event	$p^3(1 - p)$
LiDAR	$p^3(1 - p)$

3.2.2. Random-Missing Modality

Except for sensor damage, in real-world applications, sensor data can be partially missing due to temporary obstructions, noise, or other random factors. In this scenario, a certain proportion of each modality's data is zeroed out, rather than completely missing a modality. Such a condition reasonably models the unpredictability of sensor failures.

To evaluate the model's performance under random missing modalities, similar to Section 3.2.1, we define $mIoU_{RMM}^{Avg}$ and $mIoU_{RMM}^E$ to measure the model's ability with random missing modality. For each modality m_i , a proportion r of the data is randomly set to zero, where r reflects the proportion of missing data for modality m_i . We define the random-missing modality combinations as $\{M''_1, M''_2, \dots, M''_N\} \subseteq M$, where each M''_j is a combination that is made up of the modalities partly zeroed.

Table 3. Comparison of MMSS methods under EMM condition of different missing modality combinations (RD means RGB and Depth are the normal modalities).

Model	Backbone	R	D	E	L	RD	RE	RL	DE	DL	EL	RDE	RDL	REL	DEL	RDEL
CMNeXt [40]	MiT-B2	22.50	50.59	3.16	2.86	66.33	22.92	22.50	50.80	50.83	3.15	66.27	66.38	22.92	50.98	66.33
GeminiFusion [10]	MiT-B2	15.89	54.73	1.70	1.70	66.93	16.24	15.8	54.83	54.76	1.7	66.92	66.93	16.18	54.86	66.92
MAGIC [48]	MiT-B2	42.72	58.39	1.90	1.62	66.10	42.79	42.72	58.44	58.39	1.90	66.11	66.10	42.80	58.44	66.10
MAGIC++ [46]	MiT-B2	41.10	58.12	2.14	1.64	67.33	41.13	41.13	58.32	58.12	2.15	67.35	67.33	41.17	58.31	67.34
StitchFusion [13]	MiT-B2	30.93	55.44	1.87	1.59	68.22	31.03	33.55	55.76	55.41	1.87	68.23	68.21	33.66	55.71	68.20

Table 4. Comparison of MMSS methods under RMM condition of different missing modality combinations ($r = 0.75$)(RD means RGB and Depth are the normal modalities).

Model	Backbone	R	D	E	L	RD	RE	RL	DE	DL	EL	RDE	RDL	REL	DEL	RDEL
CMNeXt [40]	MiT-B2	30.05	56.34	7.04	7.16	66.26	29.98	30.12	56.54	56.39	7.07	66.28	66.32	30.06	56.61	66.33
GeminiFusion [10]	MiT-B2	22.56	58.1	2.34	2.34	66.99	22.27	22.57	58.05	58.08	2.34	66.98	66.94	22.25	58.03	66.92
MAGIC [48]	MiT-B2	42.77	58.70	3.03	2.83	66.10	42.85	42.77	58.76	58.70	3.02	66.10	66.10	42.86	58.76	66.10
MAGIC++ [46]	MiT-B2	41.22	59.97	10.52	10.30	67.33	41.20	41.25	60.15	59.97	10.59	67.34	67.33	41.23	60.15	67.34
StitchFusion [13]	MiT-B2	37.18	57.79	6.71	7.18	68.24	37.26	38.51	58.01	57.91	7.27	68.23	68.21	38.57	58.12	68.21

Table 5. Comparison of MMSS methods under RMM condition of different missing modality combinations ($r = 0.5$).

Model	Backbone	R	D	E	L	RD	RE	RL	DE	DL	EL	RDE	RDL	REL	DEL	RDEL
CMNeXt [40]	MiT-B2	38.26	58.94	19.26	19.32	66.29	38.26	38.26	59.03	59.09	19.32	66.30	66.32	38.26	59.04	66.33
GeminiFusion [10]	MiT-B2	29.33	59.48	4.38	4.41	67.01	29.22	29.37	59.53	59.55	4.35	66.98	66.93	29.21	59.48	66.92
MAGIC [48]	MiT-B2	42.90	60.55	14.87	14.78	66.10	42.94	42.91	60.58	60.53	14.81	66.10	66.10	42.95	60.57	66.10
MAGIC++ [46]	MiT-B2	42.13	61.54	18.46	18.51	67.33	42.1	42.17	61.63	61.52	18.45	67.34	67.33	42.13	61.60	67.34
StitchFusion [13]	MiT-B2	41.21	59.46	15.78	15.80	68.22	41.28	41.96	59.62	59.52	15.89	68.21	68.20	41.97	59.60	68.19

Table 6. Comparison of MMSS methods under RMM condition of different missing modality combinations ($r = 0.25$)

Model	Backbone	R	D	E	L	RD	RE	RL	DE	DL	EL	RDE	RDL	REL	DEL	RDEL
CMNeXt [40]	MiT-B2	47.71	60.92	34.61	34.67	66.31	47.78	47.75	60.94	61.01	34.73	66.31	66.32	47.77	60.98	66.33
GeminiFusion [10]	MiT-B2	44.45	61.2	18.61	18.66	66.98	44.41	44.42	61.28	61.21	18.46	66.98	66.93	44.41	61.24	66.92
MAGIC [48]	MiT-B2	43.96	61.98	28.62	28.62	66.10	43.97	43.96	62.04	61.99	28.68	66.10	66.10	43.96	62.01	66.10
MAGIC++ [46]	MiT-B2	47.06	62.83	33.23	33.16	67.33	47.06	47.07	62.88	62.83	33.30	67.34	67.33	47.10	62.89	67.34
StitchFusion [13]	MiT-B2	47.19	61.47	29.26	29.44	68.24	47.13	47.38	61.53	61.55	29.48	68.24	68.25	47.45	61.61	68.25

$mIoU_{RMM}^{Avg}$ and $mIoU_{RMM}^E$ are calculated as Eq. 4 and 5. $mIoU_{M_j''}(r_j)$ represents the validation mIoU for modality combination M_j'' with r proportion of its data missing, using model weights derived from training with the complete modality combination. When validating, the modality that is not included in M_j'' remains unchanged. In Eq. 5, p refers to the probability of each modality for random-missing, which also follows a Bernoulli distribution as Eq. 2.

$$mIoU_{RMM}^{Avg} = \frac{1}{N} \sum_{j=1}^N mIoU_{M_j''}(r), \quad (4)$$

$$mIoU_{RMM}^E(p) = \sum_{k=0}^{n-1} \sum_{j=1}^n P_p(M_j''^k) \cdot mIoU_{M_j''}. \quad (5)$$

3.2.3. Noisy Modality

In real-world applications, noise interference is inevitable. Thus, evaluating model robustness under noisy conditions is essential, which can help to ensure its reliability in practical

applications. To simulate the real world, we introduce 2 common noises: Gaussian noise and salt-and-pepper noise.

Gaussian noise N_G is used to simulate electronic sensor noise (e.g., CMOS thermal noise) and random disturbances during transmission. Because it is global, continuous, and smooth, Gaussian noise provides a realistic approximation of noise in real-world images evenly distributed across all pixels of the image, resulting in a smooth degradation of image quality. The probability density function of N_G is shown in Eq. 6, which is determined by σ and μ .

$$f(x) = \frac{1}{\sigma\sqrt{2\pi}} e^{-\frac{(x-\mu)^2}{2\sigma^2}}. \quad (6)$$

Salt-And-Pepper noise N_{SP} is used to simulate scenarios such as sensor dead pixels, data transmission errors, and dust occlusion. Unlike Gaussian noise, salt-And-Pepper noise is local, discrete, and sharp, effectively reflecting the impact of these issues on the image. N_{SP} is characterized by random extreme pixels appearing in the image, usually black (pepper) and white (salt), which makes the image visually distorted. In validation, the noisy density of N_{SP}

Table 7. EMM evaluation results.

Model	$mIoU_{EMM}^{Avg}$	$mIoU_{EMM}^E$ ($p = 0.2$)	$mIoU_{EMM}^E$ ($p = 0.1$)	$mIoU_{EMM}^E$ ($p = 0.05$)
CMNeXt [40]	37.90	54.46	60.41	63.38
GeminiFusion [10]	37.07	54.33	60.62	63.77
MAGIC [48]	44.97	58.66	62.68	64.47
MAGIC++ [46]	44.85	59.18	63.52	65.50
StitchFusion [13]	41.98	58.02	63.29	65.80

Table 8. RMM evaluation results ($r = 0.75$).

Model	$mIoU_{RMM}^{Avg}$	$mIoU_{RMM}^E$ ($p = 0.2$)	$mIoU_{RMM}^E$ ($p = 0.1$)	$mIoU_{RMM}^E$ ($p = 0.05$)
CMNeXt [40]	42.17	56.66	61.60	63.99
GeminiFusion [10]	39.78	55.88	61.47	64.22
MAGIC [48]	45.30	58.77	62.72	64.49
MAGIC++ [46]	47.06	59.81	63.78	65.62
StitchFusion [13]	45.16	59.44	64.02	66.17

Table 9. RMM evaluation results ($r = 0.5$).

Model	$mIoU_{RMM}^{Avg}$	$mIoU_{RMM}^E$ ($p = 0.2$)	$mIoU_{RMM}^E$ ($p = 0.1$)	$mIoU_{RMM}^E$ ($p = 0.05$)
CMNeXt [40]	47.49	58.85	62.68	64.53
GeminiFusion [10]	42.41	57.30	62.25	64.62
MAGIC [48]	48.19	59.53	63.01	64.61
MAGIC++ [46]	49.31	60.50	64.07	65.75
StitchFusion [13]	48.33	60.58	64.53	66.41

Table 10. RMM evaluation results ($r = 0.25$).

Model	$mIoU_{RMM}^{Avg}$	$mIoU_{RMM}^E$ ($p = 0.2$)	$mIoU_{RMM}^E$ ($p = 0.1$)	$mIoU_{RMM}^E$ ($p = 0.05$)
CMNeXt [40]	53.61	61.28	63.86	65.11
GeminiFusion [10]	49.74	60.55	63.91	65.46
MAGIC [48]	51.61	60.46	60.37	64.76
MAGIC++ [46]	53.92	62.07	64.78	66.08
StitchFusion [13]	53.10	62.34	65.39	66.85

is defined as D . During validation, some adjustments are applied to better simulate the real world: 1. Considering that the event stream is asynchronous, there will be no N_G in the event data in practical applications. Thus, to event data, N_G is not applied. 2. Considering that the commonly used definition of N_{SP} noise is based on RGB data, the black and white values in N_{SP} are defined as the maximum and minimum values for the data of other modalities. We define $mIoU_{NM}$ to evaluate the model’s ability under noisy modalities, which is the validation mIoU with model weights derived from training using the noise-free modality. With the origin input as X , the noisy input X_N with $mIoU_{NM}$ is defined as Eq. 7.

$$X_N = X + N_G(\sigma, \mu) + N_{SP}(D). \quad (7)$$

4. Experiments

4.1. Experimental Details

All experiments are conducted on 1 A800 GPU with a batch size of 4. Same as [40], we validate the models with the

image size set 1024×1024 . To verify the conjectures in Section 2.2 and ensure the comprehensiveness of the experiment, we select the representative methods of the three types of MMSS methods mentioned in Section 2.2 for validation. In more detail, we choose CMNeXt [40] for Type①, MAGIC [48], MAGIC++ [46] for Type②, and GeminiFusion [10], StitchFusion [13] for Type③. For a fair comparison, MiT-B2 [34] is selected as the backbone.

For the Entire-Missing Modality (EMM) condition, we first validate the mIoU of each possible combination for the subsequent calculations. The calculation of $mIoU_{EMM}^{Avg}$ follows Eq. 1. For $mIoU_{EMM}^E$, we set p to 3 different values: 0.2, 0.1, and 0.05, representing the different frequencies at which the damage occurs. For the Random-Missing Modality (RMM) condition, the experimental settings are the same as EMM, with p' set to the same values as p . However, when validating in the RMM condition, another hyper-parameter r exists, which reflects the proportion of data missing. For the sake of experimental completeness, we set up three degrees of data missing based on the value of r . In more detail, $r = 0.75$ refers to a high level of data missing, $r = 0.5$ refers to a middle level of data missing, and $r = 0.25$ refers to a low level of data missing. For the Noisy Modality (NM) condition, we validate the model on the RGB-Depth-Event-LiDAR modality combination. Similar to RMM, we set up three degrees of data noise based on the values of D and σ . $D = 0.2, \sigma = 0.5$ refers to a high level of data missing, $D = 0.1, \sigma = 0.2$ refers to a middle level of data missing, and $D = 0.05, \sigma = 0.1$ refers to a low level of data missing. The μ is set to 0. Expected values are additionally normalized at the end to achieve a fair comparison of indicators.

4.2. Experimental Results

4.2.1. Entire-Missing Modality

The results of EMM validation are shown in Table 3, 7 and Fig. 3. In the EMM condition, some of modalities are dropped, allowing a direct validation of each modality’s contribution and models’ robustness. Firstly, as shown in Table 3, the CMNeXt meets a huge decrease when the RGB modality is gone. For example, when it comes to DE, DL, and DEL combinations, the mIoU goes down by 15.53%, 15.50%, and 15.35%, which are the most significant decreases among the 5 models. Such results prove that Type① models rely too much on the RGB modality, which causes the potential risk when RGB cameras are broken or disturbed. Thus, the first conjecture in Section 2.2 can be initially proved. Secondly, even if the MAGIC and MAGIC++ don’t achieve the greatest mIoU under the RDEL combination, these 2 Type③ models show a surprising robustness in the EMM condition. MAGIC++ achieves the best $mIoU_{EMM}^{Avg}$, $mIoU_{EMM}^E(p = 0.2)$, and $mIoU_{EMM}^E(p = 0.1)$, while MAGIC achieves the second

Table 11. NM evaluation results.

Class	CMNeXt [40]			GeminiFusion [10]			MAGIC [48]			MAGIC++ [46]			StitchFusion [13]		
	Low	Mid.	High	Low	Mid.	High	Low	Mid.	High	Low	Mid.	High	Low	Mid.	High
Building	54.46	6.39	0	0	0	0	45.88	28.22	9.58	59.04	41.54	16.42	51.72	26.35	3.84
Fence	12.11	4.88	1.27	0.21	0	0	13.60	4.55	0.03	5.85	1.53	0.75	12.48	7.90	1.91
Other	0	0	0	0	0	0	0	0	0	0	0	0	0	0	0
Pedestrian	32.85	14.10	0.07	0.14	0	0	16.38	6.99	0.12	24.32	16.54	6.15	17.38	9.43	2.17
Pole	45.34	24.70	4.29	6.74	0.21	0	12.60	2.70	0.02	26.05	13.46	5.06	14.84	6.17	1.32
RoadLine	43.74	18.88	1.25	0.01	0	0	54.38	37.39	15.12	62.53	48.58	30.57	48.90	35.49	22.21
Road	87.94	56.83	3.00	2.54	0	0	75.74	61.59	49.11	91.85	78.38	68.66	79.10	68.19	51.83
SideWalk	52.54	27.61	5.11	0.23	0	0	39.26	14.25	0.11	47.56	32.43	8.09	35.57	24.91	10.31
Vegetation	34.46	10.34	5.60	8.96	8.27	7.48	16.91	12.77	1.21	31.23	9.89	10.73	43.20	32.35	16.84
Cars	51.99	26.13	0.14	0.04	0	0	48.73	31.42	1.00	53.99	26.65	14.37	41.69	31.69	21.36
Wall	4.72	0.15	0.01	0	0	0	21.49	8.69	0.25	21.52	7.54	1.00	10.83	4.80	2.42
TrafficSign	27.39	6.22	0.04	0.01	0	0	9.94	5.90	2.31	15.88	6.84	0.60	10.31	4.33	0.70
Sky	95.43	47.66	7.81	97.65	94.17	74.96	41.01	17.97	10.22	75.31	9.84	1.18	89.21	76.61	40.11
Ground	2.17	0.39	0	0	0	0	1.75	0.80	0.00	0.64	1.21	0.69	0.74	0.76	0.21
Bridge	4.03	0.23	0	0	0	0	10.24	2.37	0.01	36.19	24.40	1.70	11.07	2.50	2.15
RailTrack	20.78	0.39	0	0	0	0	0.78	0.41	0.21	24.51	6.80	0.40	10.81	3.36	1.47
GroundRail	9.39	2.08	0.13	0.04	0	0	8.52	2.67	0.07	13.28	7.88	4.26	9.26	4.01	0.88
TrafficLight	48.61	25.85	2.93	3.42	0.01	0	25.87	8.20	0.90	46.87	24.93	3.52	27.99	9.90	1.60
Static	14.51	1.94	0.01	0	0	0	8.58	2.58	0.05	12.3	5.47	2.02	8.35	3.72	1.16
Dynamic	5.71	0.64	0	0	0	0	2.96	0.94	0	5.55	2.30	0.15	3.87	0.94	0
Water	33.43	19.92	2.13	6.35	0	0	5.14	2.97	0.34	3.90	1.79	0.49	0.05	0.01	0
Terrain	48.80	26.52	13.12	10.06	0.88	0	29.26	17.43	2.64	42.75	22.17	6.88	33.76	20.54	5.45
TwoWheeler	17.54	5.40	0	0	0	0	17.22	5.93	0	14.00	6.86	2.16	16.78	10.82	1.49
Bus	60.42	32.25	0.39	0.18	0	0	37.79	28.11	5.93	53.28	31.44	20.52	36.69	38.30	38.37
Truck	72.42	49.64	10.45	1.49	0	0	56.60	27.94	0.30	59.52	29.19	11.01	8.20	4.76	3.40
$mIoU_{NM}$	35.23	16.37	2.31	5.52	4.14	3.30	24.03	13.31	3.98	33.12	18.31	8.70	24.91	17.11	9.25

best $mIoU_{EMM}^{Avg}$ and $mIoU_{EMM}^E (p = 0.2)$. Thus, it can be proved that the adaptive selection methods in Type③ models effectively compress the fail modality’s influence on the entire model, which is the third conjecture in Section 2.2. Thirdly, as to the Type② models, GeminiFusion achieves a similar ability to CMNeXt while StitchFusion surpasses CMNeXt but still falls behind MAGIC and MAGIC++. The fusion strategy of Type② models is effective in avoiding too much reliance on some specific modalities, while it works little to help restrain the failed modality’s influence, which is the same as the second conjecture in Section 2.2.

4.2.2. Random-Missing Modality

The results of RMM validation are shown in Table 4, 5, 6, 8, 9, and 10. As shown in Table 4, 5, and 6, StitchFusion performs better in certain modality combinations, especially consistently outperforming MAGIC in RD combinations, indicating that it has an advantage in dealing with specific modality combinations. Meanwhile, MAGIC++ is stable in most modality combinations. As the proportion of missing

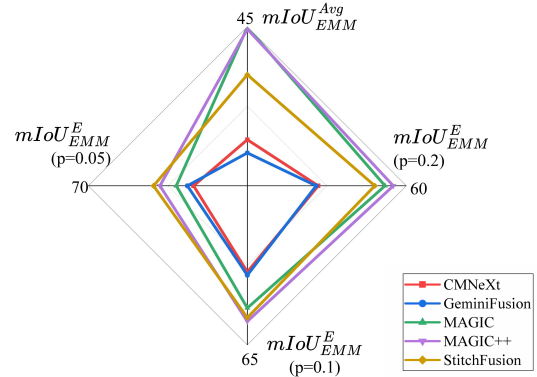


Figure 3. Visualization of EMM validation results. The scale of the radar chart is set to 5.

decreases, the performance of both methods improves significantly, especially in the case of combinations including more modalities. StitchFusion has certain advantages when dealing with more modalities, and may be more suitable for

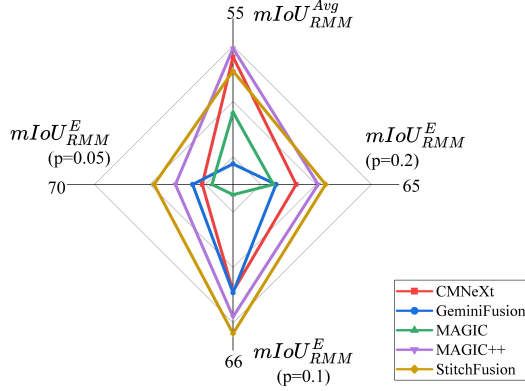


Figure 4. Visualization of RMM validation results with $r = 0.25$. The scale of the radar chart is set to 2.

scenarios where modality is less lost. MAGIC++ shows an advantage when the modality is severely lost.

As shown in Table 8, 9, 10, and Fig. 4, $mIoU_{RMM}^{Avg}$ of MAGIC++ is slightly higher than that of StitchFusion at all proportions of data missing, showing its superiority in the case of RMM. As the p value decreases, the $mIoU_{RMM}^E$ of both models shows an upward trend. StitchFusion’s $mIoU$ growth is slightly larger at low p values, especially when $p = 0.05$, StitchFusion’s $mIoU$ slightly outperforms MAGIC++.

4.2.3. Noisy Modality

As shown in Table 11, the NM validation results differ significantly between different models. CMNeXt’s $mIoU_{NM}$ ranks first when the noisy level is low, achieving 35.23%. However, when the noisy level goes up, $mIoU_{NM}$ goes through the most significant decrease, with 16.37% at the middle level and 2.31% at the high level. Such a phenomenon is most likely due to CMNeXt’s over-reliance on RGB modality. The RGB modality is a relatively information-intensive and robust modality. Thus, when the noise keeps a low level, the RGB modality is able to correct noise in other modalities. When the RGB modality collapses due to noise, the entire model quickly collapses with it. Meanwhile, GeminiFusion shows surprisingly poor performance. We believe that this is due to the excessive inter-modal information exchange in the model architecture, which leads to the continuous propagation of noise in the model, thus expanding the influence of noise on the modality. In addition, the MAGIC++ shows a relatively stable and leading performance in the NM condition. Such a finding once again proves the excellent ability of the Type③ model in terms of MMSS robustness.

4.3. More Discussions

As shown in Table 3, 4, 5, and 6, Event and LiDAR modalities appear to be relatively redundant. For example, in Table 3, the $mIoU$ of RD, RDE, RDL, and RDEL are almost

the same. For CMNeXt, the $mIoU$ of REDL is 66.33%, while the $mIoU$ of RDL is 0.05% higher. For StitchFusion, the $mIoU$ of RDEL is 68.20%, while the $mIoU$ of RD is 0.02% higher. Moreover, the contributions of Depth and LiDAR modalities seem highly similar. For example, in Table 3, the $mIoU$ of RE and RL, RDE, and RDL are almost the same across all models. Such findings suggest that the MMSS model can be optimized by reducing the redundancy between Event and LiDAR modalities. This can be achieved through feature fusion or attention mechanisms, emphasizing the unique contribution of each modality while minimizing overlap. In addition, understanding the redundancy between Event and LiDAR can guide sensor deployment decisions in real-world applications, potentially reducing costs by selectively using one modality over the other without significant performance loss.

5. Conclusion

In this study, we create a comprehensive benchmark of robustness in Multi-Modal Semantic Segmentation (MMSS), which is essential for the related models’ successful deployment in real-world scenarios characterized by uncertain data quality. This benchmark evaluates models under three challenging scenarios: Entire-Missing Modality (EMM), Random-Missing Modality (RMM), and Noisy Modality (NM). To further enhance the robustness evaluation, we model modality failure events from a probabilistic perspective, considering two key conditions: equal probability for each damaged modality combination and modality damage following a Bernoulli distribution. Based on these assumptions, we have developed four metrics ($mIoU_{EMM}^{Avg}$, $mIoU_{EMM}^E$, $mIoU_{RMM}^{Avg}$, $mIoU_{RMM}^E$) to provide a more reasonable assessment of model performance in EMM and RMM scenarios. Our work represents a pioneering effort to establish a robustness benchmark for MMSS, offering valuable insights and a foundation for future research in this field. By bridging the gap between theory and application, we aim to facilitate the development of more resilient MMSS models that can effectively handle the complexities of real-world multi-modal systems.

Acknowledgement

This work was supported by the Guangdong Provincial Department of Education Project (Grant No.2024KQNCX028); CAAI-Ant Group Research Fund; Scientific Research Projects for the Higher-educational Institutions (Grant No.2024312096), Education Bureau of Guangzhou Municipality; Guangzhou-HKUST(GZ) Joint Funding Program (Grant No.2025A03J3957), Education Bureau of Guangzhou Municipality.

References

- [1] Tim Brödermann, David Bruggemann, Christos Sakaridis, Kevin Ta, Odysseas Liagouris, Jason Corkill, and Luc Van Gool. Muses: The multi-sensor semantic perception dataset for driving under uncertainty. In *European Conference on Computer Vision*, pages 21–38. Springer, 2025. 2
- [2] Tim Brödermann, Christos Sakaridis, Yuqian Fu, and Luc Van Gool. Cafuser: Condition-aware multimodal fusion for robust semantic perception of driving scenes. *IEEE Robotics and Automation Letters*, 2025. 2, 3
- [3] Jinming Cao, Hanchao Leng, Dani Lischinski, Daniel Cohen-Or, Changhe Tu, and Yangyan Li. Shapeconv: Shape-aware convolutional layer for indoor rgb-d semantic segmentation. In *Proceedings of the IEEE/CVF international conference on computer vision*, pages 7088–7097, 2021. 2
- [4] Lin-Zhuo Chen, Zheng Lin, Ziqin Wang, Yong-Liang Yang, and Ming-Ming Cheng. Spatial information guided convolution for real-time rgb-d semantic segmentation. *IEEE Transactions on Image Processing*, 30:2313–2324, 2021.
- [5] Xiaokang Chen, Kwan-Yee Lin, Jingbo Wang, Wayne Wu, Chen Qian, Hongsheng Li, and Gang Zeng. Bi-directional cross-modality feature propagation with separation-and-aggregation gate for rgb-d semantic segmentation. In *European conference on computer vision*, pages 561–577. Springer, 2020. 2
- [6] Fuqin Deng, Hua Feng, Mingjian Liang, Hongmin Wang, Yong Yang, Yuan Gao, Junfeng Chen, Junjie Hu, Xiyue Guo, and Tin Lun Lam. Feanet: Feature-enhanced attention network for rgb-thermal real-time semantic segmentation. In *2021 IEEE/RSJ international conference on intelligent robots and systems (IROS)*, pages 4467–4473. IEEE, 2021. 2
- [7] Alexey Dosovitskiy, German Ros, Felipe Codevilla, Antonio Lopez, and Vladlen Koltun. Carla: An open urban driving simulator. In *Conference on robot learning*, pages 1–16. PMLR, 2017. 3
- [8] Mingyuan Fan, Shenqi Lai, Junshi Huang, Xiaoming Wei, Zhenhua Chai, Junfeng Luo, and Xiaolin Wei. Rethinking bisenet for real-time semantic segmentation. In *2021 IEEE/CVF Conference on Computer Vision and Pattern Recognition (CVPR)*, pages 9716–9725, 2021. 2
- [9] Di Feng, Christian Haase-Schütz, Lars Rosenbaum, Heinz Hertlein, Claudius Glaeser, Fabian Timm, Werner Wiesbeck, and Klaus Dietmayer. Deep multi-modal object detection and semantic segmentation for autonomous driving: Datasets, methods, and challenges. *IEEE Transactions on Intelligent Transportation Systems*, 22(3):1341–1360, 2020. 1, 2
- [10] Ding Jia, Jianyuan Guo, Kai Han, Han Wu, Chao Zhang, Chang Xu, and Xinghao Chen. Geminifusion: Efficient pixel-wise multimodal fusion for vision transformer. In *Forty-first International Conference on Machine Learning*. 2, 3, 5, 6, 7
- [11] Zhenchao Jin, Bin Liu, Qi Chu, and Nenghai Yu. Isnet: Integrate image-level and semantic-level context for semantic segmentation. In *2021 IEEE/CVF International Conference on Computer Vision (ICCV)*, pages 7169–7178, 2021. 2
- [12] Sanket Kachole, Xiaoqian Huang, Fariborz Baghaei Naeini, Rajkumar Muthusamy, Dimitrios Makris, and Yahya Zweiri. Bimodal segnet: Instance segmentation fusing events and rgb frames for robotic grasping. *arXiv preprint arXiv:2303.11228*, 2023. 2
- [13] Bingyu Li, Da Zhang, Zhiyuan Zhao, Junyu Gao, and Xuelong Li. Stitchfusion: Weaving any visual modalities to enhance multimodal semantic segmentation. *arXiv preprint arXiv:2408.01343*, 2024. 2, 3, 5, 6, 7
- [14] Gongyang Li, Yike Wang, Zhi Liu, Xinpeng Zhang, and Dan Zeng. Rgb-t semantic segmentation with location, activation, and sharpening. *IEEE Transactions on Circuits and Systems for Video Technology*, 33(3):1223–1235, 2022. 2
- [15] Yupeng Liang, Ryosuke Wakaki, Shohei Nobuhara, and Ko Nishino. Multimodal material segmentation. In *Proceedings of the IEEE/CVF Conference on Computer Vision and Pattern Recognition*, pages 19800–19808, 2022. 2, 3
- [16] Chenfei Liao, Xu Zheng, Yuanhuiyi Lyu, Haiwei Xue, Yihong Cao, Jiawen Wang, Kailun Yang, and Xuming Hu. Memorysam: Memorize modalities and semantics with segment anything model 2 for multi-modal semantic segmentation. *arXiv preprint arXiv:2503.06700*, 2025. 2, 3
- [17] Jiaying Liu, Dejia Xu, Wenhan Yang, Minhao Fan, and Haofeng Huang. Benchmarking low-light image enhancement and beyond. *International Journal of Computer Vision*, 129:1153–1184, 2021. 1
- [18] Ruiping Liu, Jiaming Zhang, Kunyu Peng, Yufan Chen, Ke Cao, Junwei Zheng, M. Saquib Sarfraz, Kailun Yang, and Rainer Stiefelhagen. Fourier prompt tuning for modality-incomplete scene segmentation. In *2024 IEEE Intelligent Vehicles Symposium (IV)*, pages 961–968, 2024. 2, 3
- [19] Wenyu Liu, Wentong Li, Jianke Zhu, Miaomiao Cui, Xuan-song Xie, and Lei Zhang. Improving nighttime driving-scene segmentation via dual image-adaptive learnable filters. *IEEE Transactions on Circuits and Systems for Video Technology*, 2023. 1
- [20] Yujian Mo, Yan Wu, Xinneng Yang, Feilin Liu, and Yujun Liao. Review the state-of-the-art technologies of semantic segmentation based on deep learning. *Neurocomputing*, 493: 626–646, 2022. 1, 2
- [21] Huihui Pan, Yuanduo Hong, Weichao Sun, and Yisong Jia. Deep dual-resolution networks for real-time and accurate semantic segmentation of traffic scenes. *IEEE Transactions on Intelligent Transportation Systems*, 24(3):3448–3460, 2023. 2
- [22] Adam Paszke, Abhishek Chaurasia, Sangpil Kim, and Eugenio Culurciello. Enet: A deep neural network architecture for real-time semantic segmentation. *arXiv preprint arXiv:1606.02147*, 2016.
- [23] Juncai Peng, Yi Liu, Shiyu Tang, Yuying Hao, Luta Chu, Guowei Chen, Zewu Wu, Zeyu Chen, Zhiliang Yu, Yuning Du, et al. Pp-liteseg: A superior real-time semantic segmentation model. *arXiv preprint arXiv:2204.02681*, 2022.
- [24] Rudra PK Poudel, Stephan Liwicki, and Roberto Cipolla. Fast-scnn: Fast semantic segmentation network. *arXiv preprint arXiv:1902.04502*, 2019. 2

- [25] Daniel Seichter, Mona Köhler, Benjamin Lewandowski, Tim Wengefeld, and Horst-Michael Gross. Efficient rgb-d semantic segmentation for indoor scene analysis. In *2021 IEEE international conference on robotics and automation (ICRA)*, pages 13525–13531. IEEE, 2021. 2
- [26] Kechen Song, Ying Zhao, Liming Huang, Yunhui Yan, and Qinggang Meng. Rgb-t image analysis technology and application: A survey. *Engineering Applications of Artificial Intelligence*, 120:105919, 2023. 1, 2
- [27] Changshuo Wang, Chen Wang, Weijun Li, and Haining Wang. A brief survey on rgb-d semantic segmentation using deep learning. *Displays*, 70:102080, 2021. 1, 2
- [28] Jian Wang, Chenhui Gou, Qiman Wu, Haocheng Feng, Junyu Han, Errui Ding, and Jingdong Wang. Rtformer: Efficient design for real-time semantic segmentation with transformer. In *2022 Conference on Neural Information Processing Systems (NeurIPS)*, pages 7423–7436, 2022. 2
- [29] Jiawen Wang, Chenfei Liao, Zhongqi Zhao, Lianghui Li, Xuan Gao, Suna Pan, Fangzhen Shi, Yudong Wang, Weijie Zhou, and Kehu Yang. Umsss: A visual scene semantic segmentation dataset for underground mines. In *ICASSP 2025-2025 IEEE International Conference on Acoustics, Speech and Signal Processing (ICASSP)*, pages 1–5. IEEE, 2025. 1
- [30] Yikai Wang, Xinghao Chen, Lele Cao, Wenbing Huang, Fuchun Sun, and Yunhe Wang. Multimodal token fusion for vision transformers. In *Proceedings of the IEEE/CVF conference on computer vision and pattern recognition*, pages 12186–12195, 2022. 2, 3
- [31] Wei Wu, Tao Chu, and Qiong Liu. Complementarity-aware cross-modal feature fusion network for rgb-t semantic segmentation. *Pattern Recognition*, 131:108881, 2022. 2
- [32] Bochen Xie, Yongjian Deng, Zhanpeng Shao, and Youfu Li. Eisnet: A multi-modal fusion network for semantic segmentation with events and images. *IEEE Transactions on Multimedia*, 2024. 2
- [33] Enze Xie, Wenhai Wang, Zhiding Yu, Anima Anandkumar, Jose M. Alvarez, and Ping Luo. Segformer: Simple and efficient design for semantic segmentation with transformers. In *2021 Conference on Neural Information Processing Systems (NeurIPS)*, pages 12077–12090, 2021. 2
- [34] Enze Xie, Wenhai Wang, Zhiding Yu, Anima Anandkumar, Jose M Alvarez, and Ping Luo. Segformer: Simple and efficient design for semantic segmentation with transformers. *Advances in neural information processing systems*, 34: 12077–12090, 2021. 6
- [35] Bowen Yao, Yongjian Deng, Yuhan Liu, Hao Chen, Youfu Li, and Zhen Yang. Sam-event-adapter: Adapting segment anything model for event-rgb semantic segmentation. In *2024 IEEE International Conference on Robotics and Automation (ICRA)*, pages 9093–9100. IEEE, 2024. 2
- [36] Bowen Yin, Xuying Zhang, Zhongyu Li, Li Liu, Ming-Ming Cheng, and Qibin Hou. Dformer: Rethinking rgb-d representation learning for semantic segmentation. *arXiv preprint arXiv:2309.09668*, 2023. 2
- [37] Changqian Yu, Jingbo Wang, Chao Peng, Changxin Gao, Gang Yu, and Nong Sang. Bisenet: Bilateral segmentation network for real-time semantic segmentation. In *2018 European conference on computer vision (ECCV)*, pages 325–341, 2018. 2
- [38] Changqian Yu, Changxin Gao, Jingbo Wang, Gang Yu, Chunhua Shen, and Nong Sang. Bisenet v2: Bilateral network with guided aggregation for real-time semantic segmentation. *International Journal of Computer Vision*, 129: 3051–3068, 2021. 2
- [39] Jiaming Zhang, Kailun Yang, and Rainer Stiefelwagen. Is-safe: Improving semantic segmentation in accidents by fusing event-based data. In *2021 IEEE/RSJ International Conference on Intelligent Robots and Systems (IROS)*, pages 1132–1139. IEEE, 2021. 2
- [40] Jiaming Zhang, Ruiping Liu, Hao Shi, Kailun Yang, Simon Reiß, Kunyu Peng, Haodong Fu, Kaiwei Wang, and Rainer Stiefelwagen. Delivering arbitrary-modal semantic segmentation. In *Proceedings of the IEEE/CVF Conference on Computer Vision and Pattern Recognition*, pages 1136–1147, 2023. 2, 3, 5, 6, 7
- [41] Qingyang Zhang, Yake Wei, Zongbo Han, Huazhu Fu, Xi Peng, Cheng Deng, Qinghua Hu, Cai Xu, Jie Wen, Di Hu, et al. Multimodal fusion on low-quality data: A comprehensive survey. *arXiv preprint arXiv:2404.18947*, 2024. 1
- [42] Yu Zhang and Lin Zhang. A generative adversarial network approach for removing motion blur in the automatic detection of pavement cracks. *Computer-Aided Civil and Infrastructure Engineering*, 2024. 1
- [43] Yifei Zhang, Désiré Sidibé, Olivier Morel, and Fabrice Mériaudeau. Deep multimodal fusion for semantic image segmentation: A survey. *Image and Vision Computing*, 105: 104042, 2021. 1, 2
- [44] Shenlu Zhao, Yichen Liu, Qiang Jiao, Qiang Zhang, and Jungong Han. Mitigating modality discrepancies for rgb-t semantic segmentation. *IEEE Transactions on Neural Networks and Learning Systems*, 2023. 2
- [45] Xu Zheng, Yexin Liu, Yunfan Lu, Tongyan Hua, Tianbo Pan, Weiming Zhang, Dacheng Tao, and Lin Wang. Deep learning for event-based vision: A comprehensive survey and benchmarks. *arXiv preprint arXiv:2302.08890*, 2023. 1, 2
- [46] Xu Zheng, Yuanhuiyi Lyu, Lutao Jiang, Jiazhou Zhou, Lin Wang, and Xuming Hu. Magic++: Efficient and resilient modality-agnostic semantic segmentation via hierarchical modality selection. *arXiv preprint arXiv:2412.16876*, 2024. 2, 3, 5, 6, 7
- [47] Xu Zheng, Yuanhuiyi Lyu, and Lin Wang. Learning modality-agnostic representation for semantic segmentation from any modalities. In *European Conference on Computer Vision*, pages 146–165. Springer, 2024. 2, 3
- [48] Xu Zheng, Yuanhuiyi Lyu, Jiazhou Zhou, and Lin Wang. Centering the value of every modality: Towards efficient and resilient modality-agnostic semantic segmentation. *arXiv preprint arXiv:2407.11344*, 2024. 2, 3, 5, 6, 7
- [49] Xu Zheng, Haiwei Xue, Jialei Chen, Yibo Yan, Lutao Jiang, Yuanhuiyi Lyu, Kailun Yang, Linfeng Zhang, and Xuming Hu. Learning robust anymodal segmentor with unimodal and cross-modal distillation. *arXiv preprint arXiv:2411.17141*, 2024. 2, 3
- [50] Wujie Zhou, Tingting Gong, Jingsheng Lei, and Lu Yu. Dbcnet: Dynamic bilateral cross-fusion network for rgb-t urban

scene understanding in intelligent vehicles. *IEEE Transactions on Systems, Man, and Cybernetics: Systems*, 2023. 2

- [51] Chenyang Zhu, Bin Xiao, Lin Shi, Shoukun Xu, and Xu Zheng. Customize segment anything model for multi-modal semantic segmentation with mixture of lora experts. *arXiv preprint arXiv:2412.04220*, 2024. 2, 3